# The Importance of Dehydration in Determining Ion Transport in Narrow Pores

The Importance of Dehydration in Determining Ion Transport in Narrow Pores
Richards, L. A. , Schaefer, A. , Richards, B. S. & Corry, B. 11-Jun-2012 In : SMALL. 8, 11, p. 1701-1709.

# The Importance of Dehydration in Determining Ion Transport in Narrow Pores

Laura A. Richards[1,2], Andrea I. Schäfer[2], Bryce S. Richards[1], Ben Corry[3*]

[1] *School of Engineering and Physical Sciences, Heriot-Watt University, Edinburgh, EH14 4AS, United Kingdom*

[2] *School of Engineering, The University of Edinburgh, Edinburgh, EH9 3JL, United Kingdom*

[3] *School of Biomedical, Biomolecular and Chemical Sciences, The University of Western Australia, Crawley, Western Australia 6009, Australia*

**Corresponding author: ben.corry@uwa.edu.au*

**Published in Small (2012), 8, 1701-1709**

**Abstract**

The transport of hydrated ions through narrow pores is important for a number of processes such as the desalination and filtration of water and the conductance of ions through biological channels. Here, molecular dynamics simulations were used to systematically examine the transport of anionic drinking water contaminants (fluoride, chloride, nitrate and nitrite) through pores ranging in effective radius from 2.8 to 6.5 Å to elucidate the role of hydration in excluding these species during nanofiltration. Bulk hydration properties (hydrated size and coordination number) were determined for comparison with the situations inside the pores. Free energy profiles for ion transport through the pores showed energy barriers depend on pore size, ion type, and membrane surface charge and that the selectivity sequence can change depending on the pore size. Ion coordination numbers along the trajectory showed that partial dehydration of the transported ion was the main contribution to the energy barriers. Ion transport was greatly hindered when the effective pore radius was smaller than the hydrated radius, as the ion had to lose some associated water molecules to enter the pore. Small energy barriers were still observed when pore sizes were larger than the hydrated radius due to re-orientation of the hydration shell or the loss of more distant water. These results demonstrate the importance of ion dehydration in transport through narrow pores which increases the current level of mechanistic understanding of membrane based desalination and transport in biological channels.

**Keywords:** ion hydration, pore transport, nanofiltration, ion channel, molecular dynamics

## 1. Introduction



Water and ion transport through confined pores is a topic at the forefront of research efforts because of its relevance to important applications such as desalination and the understanding of biological ion channels. Desalination is a method of addressing water scarcity, a severe and pressing issue due to increasing demand and changing climate. With approximately 70% of the world's fresh water frozen in glaciers and thus unavailable[1], desalination makes effective use of the water that is available by treating seawater or saline groundwaters to levels suitable for human consumption. On the other hand, ion channels, or biological pores, are of crucial physiological importance, with over 340 human genes thought to encode ion channels[2]. Better understanding of these ion channels will give insight into cellular and system physiology which can lead to new diagnostic tests for diseases and novel drug development[2]. The common element of these processes is that they both involve the transport of partially hydrated ions through confined pores.

Desalination is commonly achieved through the use of reverse osmosis or nanofiltration, in which water is forced through semi-permeable porous membranes. Understanding the principles underlying the transport or rejection of ions is of particular interest for improving these techniques and for developing new membranes such as those containing carbon nanotubes[3-6]. Nanofiltration is often studied using models originally built on fundamental principles of hindered transport[7] and solution diffusion[8]. Currently, most nanofiltration models are based on numerically solving the extended Nernst Planck equation and include separate terms for diffusive, convective and electrostatic contributions[9-13]. Detailed effects such as concentration polarization[14] and charge adsorption inside pores[15] are now being included in transport models. These models assume that nanofiltration membranes have pores[16, 17], yet a point of controversy remains about where actual nanofiltration 'pores' lie in the spectrum between discrete pore and dense material[18].

A major limitation in current nanofiltration models is the definition of solute size because most models use ionic[19] or Stokes radius[16], but this is inherently inaccurate due to the process of hydration. Ions are hydrated by a shell of dipolar water molecules, which means that the mobile entity is the ion with its hydrated shell rather than just the bare ion[20]. Despite the fact that hydration is neglected in nanofiltration models, the importance of hydration has been demonstrated numerous times experimentally[21-26]. Ion transport is correlated with hydrated radius[21, 22] or hydration energy[22], rather than ionic radius, because ions with smaller ionic radii have higher hydration energy and larger hydrated radii which retards their transport through the membrane[21-25]. As such, it is not the ionic size that dictates transport, but the hydrated size. Further, ions with less strongly bound shells may actually detach from their hydration layer while passing through membrane[21, 26]. This has been simulated in carbon nanotube membranes, where ions were shown to have different energy barriers depending on ion type, pore size and pressure when entering hydrophobic pores as a consequence of dehydration[27, 28]. The energetic expense of chloride transport in cylindrical $Si_3N_4$ nanopores was also related to the stripping of ion hydration layers[29].

Ion hydration is also of critical importance to biological ion channels, where significant effort has been made in understanding ion transport, and the molecular basis of selectivity is due in part to the ion's hydration properties[30-33]. Specific binding sites are located in selective transport proteins which identify the ions in their partially or fully dehydrated forms. Selection depends upon how well the interactions with the protein in this binding site can compensate for the energetic cost of ion dehydration[30]. The selectivity of most classes of anion channels corresponds to the lyotropic sequence, with weakly hydrated anions (e.g. nitrate) showing a higher permeability than strongly hydrated anions (e.g. fluoride) due to the dehydration energy required for transport[34, 35]. However, the majority of work on anionic selectivity in ion channels has largely focused on chloride because chloride is the only halogen ion used in abundance in biological systems. Chloride transport is typically controlled by chloride channel transport proteins which have an hourglass-shaped chloride selectivity filter which forms a row of binding sites for the fully or partially dehydrated chloride ion [36, 37]. This filter is not highly selective between chloride and bromide[38], but this is not required in nature.

Alternatively, cation channels are highly selective and are constructed differently than the chloride channel proteins by having large aqueous vestibules within the transmembrane spanning portion of the membrane[30]. Differences in hydration are important in explaining the extremely precise selectivity in potassium channels (and other cation channels) that are up to 1000 times more permeable to potassium than sodium. Although sodium is a smaller ion, the energy required to remove the hydration shell is greater than the energy gained by interacting with the carbonyl oxygen in the channels as compared to potassium[39]. The ease of constraining a hydrated potassium ion inside a narrow pore relative to hydrated sodium or lithium is highly dependent on pore radius[40].

Hydration during pore transport processes is not well-understood (and to date completely un-addressed in nanofiltration models), for a number of reasons. Firstly, the lack of available hydration data relevant to nanofiltration is a major limitation. Determining information about hydration free energies and structure is difficult. While data exists for a variety of ions[41-43], these lists are not comprehensive[23] and there is considerable discrepancy on reported values due to differing methods and assumptions used. Data is insufficient for many drinking water contaminants, such as nitrite or nitrate. Secondly, hydration during pore transport includes complex interactions with the membrane; hence information on hydration in bulk solution cannot be applied within the pore. Thirdly, if partial or complete dehydration occurs during the process of transport[21, 26, 27], the hydrated radius is therefore a transient parameter, and very little is known about how to account for this in transport models. A more detailed approach is thus required that incorporates the interaction of water molecules with the ion as well as the interaction between the hydrated ion and the pore.

The overall aim of this study was to examine the hydration of a selection of monovalent anions relevant to drinking water purification (fluoride, chloride, nitrate ($NO_3^-$), nitrite ($NO_2^-$)) as they transport through nanopores to determine its importance in this process. The specific objectives were to: (1) determine the hydration structure of the anions in bulk water; (2) investigate the hydration of these ions during transport through a generic pore, as a function of (i) pore size; (ii) ion type; and (iii) surface charge; and (3) determine the energetic barriers of transport by evaluating free energy profiles in each of these scenarios.

The novelty in this study lies in systematically evaluating the dehydration mechanism during pore transport for small ions with molecular dynamics (MD). Rather than attempting to describe all the complexity of realistic membrane pores, we use simplified channels so as to be able to more easily isolate the role of ion dehydration in pores of different sizes. By carefully parameterizing the simulations to reproduce ion dehydration energies, many ion types and pore sizes can be examined, which would be difficult with more detailed simulations. This study provides the evidence that dehydration is the determining factor in transport of ions through these pores, and that such effects occur in conditions applicable to desalination and biological pores.

## 2. Methods

### 2.1 Parameterization

Force field parameters required for MD simulations were available for fluoride and chloride[44] but had to be specifically developed for nitrate and nitrite using *ab-initio* quantum mechanical and MD techniques[45]. Gaussian03[46] software was used to conduct geometry optimization (bond length, angle stretch and improper torsion), frequency analysis, and to calculate partial charges with the



Merz-Singh-Kollman electrostatic fitting scheme[47], all using Hartree Fock theory and a 6-31+G* basis set. Force constants were determined from potential energy surface scans, and then adjusted to match the infrared spectra from a MD vacuum simulation to the infrared frequencies obtained from the Gaussian calculation. Lennard-Jones (LJ) parameters ($r_{min,ij}$ and $\varepsilon_{ij}$) for all non-bonded atoms were systematically adjusted, as described below, to reproduce the hydration free energies of the ions.

The method of alchemical free energy perturbations[45] (FEP) was used to validate the ion parameterization by calculating the overall free energy difference between two ions in bulk water and comparing to literature values[41]. A single chloride ion was placed in the center of a 40×40×40 Å TIP3P[45, 48] water box and slowly morphed into either nitrate or nitrite in 20 thermodynamic perturbation equilibration steps each lasting 500-ps. The non bonded LJ parameters were adjusted until the difference in hydration free energy of the ions was within 1 kcal.mol$^{-1}$ of the target value, which was -71.6 kcal.mol$^{-1}$ for nitrate and -78.8 kcal.mol$^{-1}$ for nitrite [41]. The final optimized parameters for each ion and a schematic for representation of the ion structure are shown in Table S1 and Figure S1, respectively.

[Table S1]

[Figure S1]

### 2.2 Model System

MD simulations were conducted for two kinds of systems using NAMD2.7[49] with the fluoride, chloride and sodium parameters of Joung and Cheatham[44], and those for nitrite and nitrate developed here, and VMD1.9 for visualization[50]. The first system was a simple box of TIP3P[45, 48] water containing the ion which was used to determine unconstrained hydrated size and structure in bulk water. Bulk simulations were minimized for 1-ps and run for 500-ps with a single ion in a water box of 60×60×60 Å (6843 water molecules) at 298 K and 1 atm (controlled with Langevin dynamics). The radial distribution function (RDF) was calculated in order to determine the structure of the hydration shell(s) around the ion. The hydrated radius ($R_{hyd}$) was defined at the first minima in the RDF. The coordination number (the number of water molecules associated with the ion) was determined from the average number of water molecules within the hydrated radius.

The second type of simulations contained a pore, which was represented as a smooth, idealized surface to be generic and avoid giving specific chemical characteristics. While the surface representation could have been achieved using analytical functions or numerical tables, closely spaced discrete atoms were selected for computational efficiency. These atoms were spaced at an interval of 1 Å as smaller spacing did not influence the LJ interaction as a function of distance from the pore wall. The interaction of water and ions with the wall was through LJ interactions defined by $r_{min,surface}$ = 3.75 Å and $\varepsilon_{surface}$ = 0.1946 kcal.mol$^{-1}$ (based upon values for methyl groups in hydrocarbon chains which is of relevance to biological and membrane pores)[51, 52]. The density of atoms on the surface was used to scale $\varepsilon_{surface}$ to reproduce methyl LJ interactions when the atoms are at the density of real methyl groups. A pore of total length 16 Å (selected to ensure that length was more than twice the widest radius) was constructed and solvated in a water box of dimensions 40×40×70 Å with periodic boundary conditions for continuity. Pressure and temperature were controlled using Langevin Dynamics. The damping coefficient for temperature control was 5-ps$^{-1}$ and the oscillation period for pressure control was 200-fs. Full-system periodic electrostatics (Ewald summation) were applied on a grid size of 75 × 75 × 90 Å. A van der Waals cutoff distance of 12 Å was specified, with switching functions used to smoothly bring the forces and energy to zero from a switching distance of 10 Å. The timestep was set to 1 fs.step$^{-1}$ as rigid bonds were not used for any atoms in the system. All systems were ionized for a net concentration of 0.1M sodium

fluoride, sodium chloride, sodium nitrate or sodium nitrite (single salt per simulation). This meant that there were five cations, five anions and approximately 2400 water molecules per simulation (for a 3.3 Å effective pore).

The effective radius of the pore available to water ($R_{eff}$) was used to define the pore radius rather than the size defined by the location of the center of the surface atoms ($R_p$) because $R_{eff}$ was more easily compared to the hydrated radius of each ion. Effective radius was determined by calculating the oxygen density profile within the pore, and adding the distance at which it became zero to the ionic radius of oxygen ($R_{ion,oxygen}$ = 1.77 Å) in water. This effective radius was always less than the position of the center of the surface atoms due to the LJ interactions between the surface atoms and water. For reference, effective radii of 2.8, 3.3, 3.7, 4.3, 5.3 and 6.5 Å correspond to surface atoms centered at $R_p$ = 4.0, 4.5, 5.0, 5.5, 6.5 and 7.5 Å. Pore radii were selected to be similar to nanofiltration membranes[53] as well those used in previous simulations of narrow carbon nanotubes[27, 28]. An additional simulation was conducted with surface atoms centered at $R_p$ = 3.0 Å but a corresponding effective radius could not be calculated because water evacuated from the pore.

The pore was neutral for all simulations with the exception of two surface charge simulations (at $R_{eff}$ = 3.3 and 4.3 Å) where a charge of -0.1 $C.m^{-2}$ was evenly distributed along all atoms on the top surface. The pore representation did not account for pore size distributions, tortuousity, and functional groups on the surface, which can be relevant to transport processes in nanofiltration, carbon nanotubes, and biological pores. Figure 1 shows a side-view representation of the model system.

[Figure 1]

The free energy (or potential of mean force) of an ion passing through the pore was determined using umbrella sampling[54] in which a harmonic potential was used to set the location of the ion of interest along a trajectory path defined by the distance from the central pore axis $r_{radial}$ and the vertical position Z. The target positions for the ion were moved from Z = -15 Å (bulk) to 0 Å (center of pore) along the pore axis ($r_{radial}$ = 0) for all pore sizes with a step size of 1Å. Additional positions were sampled from Z = -15 to 7Å (at $r_{radial}$ = 4Å) for $R_{eff}$ = 2.8 and 3.3 Å; Z = -15 to 0 Å (at $r_{radial}$ = 4 Å) for $R_{eff}$ = 3.7 and 4.3 Å; and Z = -15 to 0 Å (at $r_{radial}$ = 4Å and 8Å) for $R_{eff}$ = 5.3 and 6.5 Å. For the neutral membranes, the symmetry of the system is used to generate a potential of mean force across the entire length of the pore (-15 < Z < 15). The applied force constants were 2 $kcal.mol^{-1}.Å^{-2}$ and 0.2 $kcal.mol^{-1}.Å^{-2}$ in the Z and $r_{radial}$ directions, respectively, and were selected for complete sampling. For each target position, a 250-ps simulation was run, and the coordinate of the ion was written every 1 ps. The weighted histogram analysis method (WHAM) [55, 56] was used to calculate two-dimensional free energy profiles with a tolerance of 0.0001 and 30 bins in both Z and $r_{radial}$ directions. Two-dimensional profiles were integrated at each Z position[28] to determine a one-dimensional profile. All energy profiles were single-ion profiles as no other ions entered the pores during the simulations.

Reproducibility of the free energy calculations was estimated to be ± 0.3 $kcal.mol^{-1}$ using the Monte Carlo Bootstrap error analysis[57] feature within WHAM for fluoride at $R_{eff}$ = 2.8 Å as determined with 1000 Monte Carlo trials and correlation time of 100. This accuracy was assumed to be similar for all simulations. To further asses the uncertainty in the free energy values, seven independent trajectories were conducted for one case (fluoride at $R_{eff}$ = 3.3 Å) in order to show error of repeated simulations. The standard deviation of the peak of the energy barrier from the seven independent trajectories was ± 2.3%, and this was also assumed to be similar for all trajectories. Convergence of the simulations was further evidenced by taking the average and standard deviation of energy outputs over the last 20% of the sample windows of 500-ps (bulk simulations) and 250-ps (per umbrella window). The standard deviation as a percentage of the average value was ± 0.07% and



1.4% for the 500-ps and 250-ps simulation windows, respectively. Because the magnitude of the error bars is small, they are not marked on the figures.

## 3. Results and Discussion

### 3.1 Ion behavior in bulk water

The hydration properties of each ion in bulk water are shown in Table 1 and provide a basis of comparison for hydration properties in the pore. Fluoride had the smallest hydrated size ($R_{hyd,fluoride}$ = 3.4 Å), smallest average coordination number (6.5) and highest hydration energy (-119.7 $kcal.mol^{-1}$). Nitrate and nitrite had larger hydrated radii (5.0 Å and 5.1 Å, respectively) and more water molecules associated with them compared to the single atom ions fluoride (3.4 Å) and chloride (3.8 Å). The most weakly hydrated ion was nitrate, which had the highest average coordination number (15.5) and lowest hydration energy (-71.6 $kcal.mol^{-1}$) meaning that each water molecule was bound weakly to the ion. Note that nitrate and nitrite were not spherical ions, and thus were not spherical when hydrated because water molecules associated at highest density around the polar sites on the nitrogen and oxygen atoms. The radial distribution functions and instantaneous distributions of coordination numbers are shown in Figure S2.

[Table 1]

[Figure S2]

### 3.2 Ion transport as a function of pore size

The free energy profiles of fluoride entering pores of different sizes are shown in Figure 2A. In the narrowest pore studied ($R_p$ = 3.0 Å), water evacuated the pore during system equilibration. Such evacuation in small pores has been observed previously[51] and so this narrowest pore size was not further pursued in this study because the focus here was aimed at pore sizes that had been experimentally characterized for typical nanofiltration membranes[53]. In the remaining cases, the highest energy barrier for ion transport through the pore (46.9 $kcal.mol^{-1}$) occurred with the smallest pore where water remained during equilibration ($R_{eff}$ = 2.8 Å) because ion transport is the most hindered. The energy barrier was not simply a linear function of pore size; there was significant impact of pore size on free energy at $R_{eff}$ = 2.8, 3.3 and 3.7 Å but the impact became less prominent at the largest pore sizes $R_{eff}$ = 5.3 and 6.5 Å.

A plot of the maximum of the free energy versus pore size (Figure 2B) shows two key regimes that dictate transport. The first regime has a steep dependence of the energy barrier on pore radius and occurred at lower pore radii ($R_{eff}$ = 2.8 to 3.7 Å) where transport was highly hindered (energy barrier > 10 $kcal.mol^{-1}$). The highly hindered regime occurred when the hydrated radius (3.4 Å) was larger than or similar to the effective radius of the pore meaning that water must be stripped from the ion for it to enter the pore. At larger pore radii ($R_{eff}$ = 4.3 to 6.5 Å), transport had smaller hindrance (energy barrier < 6 $kcal.mol^{-1}$) and the slope of the curve is less because fluoride could fit into the pore with its entire first hydration shell. The dehydration energy does not scale linearly with the number of water molecules, as the first water binds most strongly to the ion. This is apparent in both ab-initio and MD calculations of binding energies[44], but is more evident in the pores where the limited space reduces hydrogen bonding between the coordinating waters as observed previously by Song and Corry, who determined the non-linearity of free energy required to partially or fully dehydration chloride in a pore[27].

[Figure 2]

A quantitative and visual analysis of coordination number (Figure 3 and 4, respectively) clearly showed that these energy barriers were due to dehydration because water molecules were removed from the hydration layer to allow fluoride to "squeeze" into the smaller pores. In the smallest pore ($R_{eff}$ = 2.8 Å), the coordination number of fluoride decreased from six to two as it moved from bulk into this pore, which means that it was partially dehydrated with the loss of four water molecules from its inner hydration shell, explaining the very large energy barrier. The coordination number remained at two with no deviation inside the pore as there was a single chain of molecules through the pore as shown in Figure 4, thus there was no other option for fluoride to coordinate with more than two water molecules once inside.

For pore sizes with effective pore size larger than the hydrated radius, fluoride did not have to dehydrate, resulting in a much smaller energy barrier for the transport. Small energy barriers at large pore sizes (for example 1.7 kcal.mol$^{-1}$ at $R_{eff}$ = 6.5 Å) were due to slight rearrangement of the hydration shell and/or losing water from the second and more distant hydration layer.

These results are reasonable when compared with energy barriers found in carbon nanotubes, nanofiltration, reverse osmosis and biological channels. The energy required to strip water from the hydration shell of sodium as it was entering a carbon nanotube was approximately 8.5 kcal.mol$^{-1}$ per water molecule[27], whereas it is approximately 10 kcal.mol$^{-1}$ per water molecule in this study for fluoride (as calculated by dividing the energy barrier by the decrease in coordination number). Energy barriers of pure water permeation in reverse osmosis and inorganic nanofiltration membranes have been reported in the range of 4.3 to 7.2 kcal.mol$^{-1}$ [59]. The physiological role of biological channels is to transport ions across a membrane and thus most narrow biological pores (such as potassium channels) contain polar groups with which the ions can interact to overcome the dehydration penalty. Biological pores with non-polar lining do exist, but must open wider to pass ions. It has been noted, for example, that the 3.0 Å radius non-polar interior of the closed state acetylcholine receptor presents a 6 kcal.mol$^{-1}$ barrier to sodium and 4 kcal.mol$^{-1}$ to chloride[27, 40, 60].

[Figure 3]

[Figure 4]

### 3.3 Ion transport as a function of ion type

The effect of ion type on transport was examined as shown in Figure 5 to assess differences in behavior according to ion properties. The free energy profiles (Figure 5A and 5B) demonstrate a strong dependence of energy barrier on ion type due to ion size, hydrated size, and hydration strength. In the smaller pore ($R_{eff}$ = 3.3 Å, Figure 5A) fluoride had the highest barrier (27.4 kcal.mol$^{-1}$), followed by chloride (21.8 kcal.mol$^{-1}$), nitrite (11.1 kcal.mol$^{-1}$) and nitrate (6.3 kcal.mol$^{-1}$). This order matched the trend in hydration energy (Table 1), showing that in a very narrow pore, the energy barriers in transport match the hydration energy trends. In the larger pore ($R_{eff}$ = 4.3 Å, Figure 5B) energy barriers decreased for all ion types, which was consistent with the behavior discussed for fluoride.

An interesting switch in the trend of the energy barriers occurred with fluoride and chloride with the two pore sizes shown in Figure 5. In the larger pore ($R_{eff}$ = 4.3 Å), chloride had the higher energy barrier, whereas fluoride was the most hindered with the smaller pore ($R_{eff}$ = 3.3 Å). Plots of the coordination numbers in the pore (Figure 5C and 5D) can be used to explain these results. In the smaller pore ($R_{eff}$ = 3.3 Å), each of the ions had to partially dehydrate: fluoride partially dehydrated from approximately seven to four associated water molecules; chloride from seven to four; nitrate from fifteen to seven; and nitrite from twelve to six. This shows that partial dehydration resulted in the energy barriers. Nitrate had the lowest energy barrier because even though it lost eight



associated waters during transport (the largest number of any of the ions), it had the most waters associated with it in the bulk (15.5) and the lowest hydration energy (-71.6 kcal.mol$^{-1}$) so the dehydration did not have a large energetic cost.

In contrast, in the larger pore size ($R_{eff}$ = 4.3 Å) partial dehydration occurred for each ion except fluoride. Fluoride was sufficiently small to fit in the pore without dehydrating (whereas chloride still needed to dehydrate), which explains the switch in fluoride and chloride between Figures 5A and 5B. This is similar to the classic idea of 'size selectivity' but is based upon the size of the hydrated rather than the bare ion or Stokes radii[61-63]. A similar switch in the order of the energy barriers has been seen for sodium and potassium[27, 40]. Fluoride did not dehydrate, chloride partially dehydrated from seven to six associated waters; nitrate from fifteen to ten, and nitrite from twelve to nine. The smaller amount of dehydration required resulted in the lower free energies at $R_{eff}$ = 4.3 Å. These results were consistent with data previously published by Song and Corry, which stated that the free energy required to partially dehydrate chloride to three associated waters was 20.3 kcal.mol$^{-1}$ and to six waters was 9.50 kcal.mol$^{-1}$ (compared to 21.8 kcal.mol$^{-1}$ at $R_{eff}$ = 3.3 Å and 7.74 kcal.mol$^{-1}$ for $R_{eff}$ = 4.3 Å in this study)[27].

[Figure 5]

### 3.4 Surface charge

Most nanofiltration membranes contain charged groups on the membrane surface, rather than being neutral, which influences ion rejection. To compare the importance of ion dehydration with the better characterized mechanism of charge repulsion, additional simulations were conducted with a repulsive charge (-0.1 C.m$^{-2}$) evenly distributed on the top surface. The magnitude of these charges was chosen to be greater than that expected in most nanofiltration situations (typical range from approximately -0.05 to +0.01 C.m$^{-2}$)[64] as to compare dehydration with charge repulsion in an extreme case.

The effect of surface charge on free energy profiles is shown in Figure 6. The inclusion of negative charge on the top surface led to a higher energy barrier compared to when charge was not considered. This is most likely caused by direct charge repulsion occurring between the negative surface and negative fluoride ion, but could also arise from interactions between water and the charged membrane or entropic changes. However, even though charge contributed by increasing the energy barrier, it is important to note that dehydration remained the dominant effect. At the smaller pore size ($R_{eff}$ = 3.3 Å) charge contributed 14% to the maximum free energy (4.5 kcal.mol$^{-1}$ of a total barrier of 31.6 kcal.mol$^{-1}$) and at $R_{eff}$ = 4.3 Å, charge contributed 20% to the maximum free energy. Charge had a larger relative effect at the larger pore sizes, because the contribution of dehydration to the total energy barrier was less. These results are important as they demonstrate that dehydration remains the dominant barrier to pore transport as compared to charge repulsion. Further investigation on the influence of pore polarity as well as charge distribution/orientation within the pore is ongoing.

[Figure 6]

## 4. Conclusions

Three key conclusions can be drawn from this work. Firstly, energetic barriers were strongly dependent on pore size. Energy barriers were not linearly correlated with pore size; instead, there were distinct regimes related to the required dehydration. Transport was strongly hindered when the size of the pore was smaller than the hydrated radius. Secondly, energy barriers depended on ion type (and hence hydration properties) and the selectivity sequence amongst the ions can change depending on the pore size. In general, the transport of small, strongly hydrated ions (such as

fluoride) was much more energetically expensive than for larger, less strongly hydrated ions (such as nitrate) due to the required dehydration unless the pore is larger than the size of the hydrated ion**.** This could have important implications in utilizing the different barriers in order to separate different types of ions, which is especially exciting from the perspective of removing contaminants other than sodium chloride in seawater desalination. Further work is ongoing to pinpoint the pore sizes that enable the best discrimination between the ion types studied, although the issue is complicated when polar groups are present in the pore walls. Thirdly, and most importantly, these results showed that dehydration was the main barrier to ion transport in the narrow pores. In particular, partial dehydration was the main determinant of the energy barriers for small, strongly hydrated ions whose hydrated radius is larger than the pore size, even when charge repulsion is considered. This explains, for example, why fluoride is rejected by membranes with pore sizes greater than the ionic radius of fluoride. Demonstrating that the process of hydration/dehydration is important in nanofiltration will encourage future models to incorporate these interactions. It may be possible, for example, to include the energetic barriers calculated in MD directly into the continuum transport models commonly used in describing nanofiltration. While MD simulations are an extremely valuable tool in understanding ion transport, it is important to note this generic model cannot exactly replicate a nanofiltration pore or membrane due to factors such as pore size distributions, tortuousity and functional groups on the membrane surface. Experimental evidence of dehydration occurring during ion transport in a nanofiltration membrane is yet to be systematically demonstrated but will provide a complementary and significant step forward in understanding this mechanism. By providing a systematic and novel insight into the role of ion dehydration in pore transport, the results obtained are significant in understanding anionic selectivity in biological channels as well as desalination and removal of various drinking water contaminants with nanofiltration.

**Acknowledgements**

The authors would like to thank IChemE, Joint Research Institute in Energy (Heriot-Watt University), the School of Engineering and Physical Sciences (Heriot-Watt University), Overseas Research Students Awards Scheme and James Watt Scholarship for financial support for Laura Richards' PhD studentship and visit to the University of Western Australia. All computation work was done using a grant under the merit allocation scheme of the National Computational Infrastructure (NCI) National Facility (Australia) and additional computer time from iVEC. Dylan Jayatilaka and Michael Thomas (University of Western Australia) are thanked for valuable discussions and Gavin Park and Graham Craik (Heriot-Watt University) and Michael Thomas for proofreading.

**Supporting Information Available:** The following additional information is provided: (i) force field parameters for fluoride, chloride, nitrate, and nitrate, (ii) a representative schematic to illustrate parameterized terms; and (iii) radial distribution functions and instantaneous coordination numbers of each ion in bulk water.

**References**

[1] I.A. Shiklomanov, J.C. Rodda, World water resources at the beginning of the twenty-first century, Cambridge University Press, 2003.
[2] M. Ashcroft, From molecule to malady, Nature, 440 (2006) 440 - 447.
[3] K.P. Lee, T.C. Arnot, D. Mattia, A review of reverse osmosis membrane materials for desalination - Development to date and future potential, Journal of Membrane Science, 370 (2011) 1 - 22.
[4] B.J. Hinds, N. Chopra, T. Rantell, R. Andrews, V. Gavalas, L.G. Bachas, Aligned multiwalled carbon nanotube membranes, Science, 303 (2004) 62 - 65.



[5] A. Kalra, S. Garde, G. Hummer, Osmotic water transport through carbon nanotube membranes, Proceedings of the National Academy of Science, 100 (2003) 10175 - 10180.
[6] D. Mattia, Y. Gogotsi, Review: static and dynamic behavior of liquids inside carbon nanotubes, Microfluid Nanofliud, 5 (2008) 289 - 305.
[7] M. Soltanieh, W.N. Gill, Review of reverse osmosis membranes and transport models, Chemical Engineering Communications, 12 (1981) 379 - 363.
[8] J.G. Wijmans, R.W. Baker, The solution-diffusion model: a review, Journal of Membrane Science, 107 (1995) 1 - 21.
[9] W.R. Bowen, J.S. Welfoot, Modelling the performance of membrane nanofiltration - critical assessment and model developmen, Chemical Engineering Science, 57 (2002) 1121 - 1137.
[10] J. Schaep, C. Vandecasteele, A.W. Mohammad, W.R. Bowen, Modelling the retention of ionic components for different nanofiltration membranes, Separation and Purification Technology, 22-23 (2001) 169-179.
[11] A. Szymczyk, P. Fievet, Investigating transport properties of nanofiltration membranes by means of a steric, electric and dielectric exclusion model, Journal of Membrane Science, 252 (2005) 77 - 88.
[12] A. Szymczyk, C. Labbez, P. Fievet, A. Vidonne, A. Foissy, J. Pagetti, Contribution of convection, diffusion and migration to electrolyte transport through nanofiltration membranes, Advances in Colloid and Interface Science, 103 (2003) 77 - 94.
[13] A.E. Childress, M. Elimelech, Relating nanofiltration membrane performance to membrane charge (electrokinetic) characteristics, Environmental Science and Technology, 34 (2000) 3710 - 3716.
[14] S. Déon, P. Dutournié, P. Bourseau, Modeling nanofiltration with Nernst-Planck approach and polarization layer, American Institute of Chemical Engineers Journal, 53 (2007) 1952 - 1969.
[15] S. Déon, A. Escoda, P. Fievet, A transport model considering charge adsorption inside pores to describe salts rejection by nanofiltration membranes, Chemical Engineering Science, 66 (2011) 2823 - 2832.
[16] W.R. Bowen, A.W. Mohammad, N. Hilal, Characterisation of nanofiltration membranes for predictive purposes - use of salts, uncharged solutes and atomic force microscopy, Journal of Membrane Science, 126 (1997) 91 - 105.
[17] J. Schaep, B. Van Der Bruggen, C. Vandecasteele, D. Wilms, Influence of ion size and charge in nanofiltration, Separation and Purification Technology, 14 (1998) 155-162.
[18] M. Nyström, L. Kaipia, S. Luque, Fouling and retention of nanofiltration membranes, Journal of Membrane Science, 98 (1995) 249-262.
[19] W.R. Bowen, H. Mukhtar, Characterisation and prediction of separation performance of nanofiltration membranes, Journal of Membrane Science, 112 (1996) 263 - 274.
[20] R.A. Robinson, R.H. Stokes, Electrolyte Solutions, Butterworth & Co., London, 1959.
[21] B. Tansel, J. Sager, T. Rector, J. Garland, R. Strayer, L. Lanfang, M. Roberts, M. Hummerick, J. Bauer, Significance of hydrated radius and hydration shells on ionic permeability during nanofiltration in dead end and cross flow modes, Separation and Purification Technology, 51 (2006) 40-47.
[22] S.M.S. Ghiu, R.P. Carnahan, M. Barger, Mass transfer in RO TFC membranes - dependence on the salt physical and thermodynamic parameters, Desalination, 157 (2003) 385 - 393.
[23] P. Mukherjee, A.K. Sengupta, Ion exchange selectivity as a surrogate indicator of relative permeability of ions in reverse osmosis processes, Environmental Science and Technology, 37 (2003) 1432 - 1440.
[24] C.T. Matos, R. Fortunato, S. Velizarou, M.A.M. Reis, J.G. Crespo, Removal of mono-valent oxyanions from water in an ion exchange membrane bioreactor: Influence of membrane permselectivity, Water Research, 42 (2008) 1785 - 1795.
[25] P.Y. Pontalier, A. Ismail, M. Ghoul, Mechanisms for the selective rejection of solutes in nanofiltration membranes, Separation and Purification Technology, 12 (1997) 175 - 181.

[26] L. Li, J. Dong, T.M. Nenoff, Transport of water and alkali metal ions through MFI zeolite membranes during reverse osmosis, Separation and Purification Technology, 53 (2007) 42 - 48.
[27] C. Song, B. Corry, Intrinsic ion selectivity of narrow hydrophobic pores, Journal of Physical Chemistry B, 113 (2009) 7642 - 7649.
[28] B. Corry, Designing carbon nanotube membranes for efficient water desalination, Journal of Physical Chemistry B, 112 (2008) 1427 - 1434.
[29] M. Zwolak, J. Lagerqvist, M. Di Ventra, Quantized Ionic Conductance in Nanopores, Physical Review Letters, 103 (2009) 128102 - 128106.
[30] E. Gouaux, R. MacKinnon, Principles of selective ion transport in channels and pumps, Science, 310 (2005).
[31] A. Miyazawa, Y. Fujiyoshi, N. Unwin, Structure and gating mechanisms of the acetylcholine receptor pore, Nature, 423 (2003) 949 - 955.
[32] Y. Zhou, J.H. Morais-Cabral, A. Kaufman, R. MacKinnon, Chemistry of ion coordination and hydration revealed by a K+ channel-Fab complex at 2.0 Å resolution, Nature, 414 (2001) 43 - 48.
[33] O. Beckstein, K. Tai, M.S.P. Sansom, Not ions alone: Barriers to ion permeation in nanopores and channels, Journal of the American Chemical Society Communications, 126 (2004) 14694 - 14695.
[34] P. Linsdell, A. Evagelidis, J.W. Hanrahan, Molecular determinants of anion selectivity in the cystic fibrosis transmembrane conductance regulator chloride channel pore, Biophysical Journal, 78 (2000) 2973 - 2982.
[35] Y. Chen, L. Hu, M. Punta, R. Bruni, B. Hillerich, B. Kloss, B. Rost, J. Love, S.A. Siegelbaum, W.A. Hendrickson, Homologue structure of the SLAC1 anion channel for closing stomata in leaves, Nature, 467 (2010) 1074 - 1080.
[36] R. Dutzler, E.B. Campbell, M. Cadene, B.T. Chait, R. MacKinnon, X-ray structure of a ClC chloride channel at 3.0 Å reveals the molecular basis of anion selectivity, Nature, 415 (2002) 287.
[37] R. Dutzler, E.B. Campbell, R. MacKinnon, Gating the selectivity filter in ClC chloride channels, Science, 300 (2003).
[38] A. Accardi, L. Kolmakova-Partensky, C. Willaims, C. Miller, Ionic currents mediated by a prokaryotic homologue of ClC $Cl^-$ channels, The Journal of General Physiology, 123 (2004) 109-119.
[39] D.A. Doyle, J.M. Cabral, R.A. Pfuetzner, A. Kuo, J.M. Gulbis, S.L. Cohen, B.T. Chait, R. MacKinnon, The Structure of the Potassium Channel: Molecular Basis of $K^+$ Conduction and Selectivity, Science, 280 (1998) 69 - 77.
[40] M. Carrillo-Tripp, M.L. San-Román, J. Hernańdez-Cobos, H. Saint-Martin, I. Ortega-Blake, Ion hydration in nanopores and the molecular basis of selectivity, Biophysical Chemistry, 124 (2006) 243 - 250.
[41] Y. Marcus, Thermodynamics of solvation of ions. Part 5: Gibbs free energy of hydration at 298.15 K, Journal of the Chemical Society, Faraday Transactions, 87 (1991) 2995 - 2999.
[42] E.R. Nightingale, Phenomenological Theory of Ion Solvation. Effective Radii of Hydrated Ions, The Journal of Physical Chemistry, 63 (1959) 1381-1387.
[43] J. Burgess, Metal ions in solution, Halsted Press, New York, 1978.
[44] I.S. Joung, T.E. Cheatham III, Determination of alkali and halide monovalent ion parameters for use in explicitly solvated biomolecular simulations, Journal of Physical Chemistry B, 112 (2008) 9020 - 9041.
[45] O.M. Becker, A.D.M. Jr, B. Roux, M. Watanabe, Computational Biochemistry and Biophysics, Marcel Dekker, New York, 2001.
[46] M.J. Frisch, G.W. Trucks, H.B. Schlegel, G.E. Scuseria, M.A. Robb, J.R. Cheeseman, J. J. A. Montgomery, T. Vreven, K.N. Kudin, J.C. Burant, J.M. Millam, S.S. Iyengar, J. Tomasi, V. Barone, B. Mennucci, M. Cossi, G. Scalmani, N. Rega, G.A. Petersson, H. Nakatsuji, M. Hada, M. Ehara, K. Toyota, R. Fukuda, J. Hasegawa, M. Ishida, T. Nakajima, Y. Honda, O. Kitao, H. Nakai, M. Klene, X. Li, J.E. Knox, H.P. Hratchian, J.B. Cross, V. Bakken, C. Adamo, J. Jaramillo, R. Gomperts, R.E. Stratmann, O. Yazyev, A.J. Austin, R. Cammi, C. Pomelli, J.W. Ochterski, P.Y.



Ayala, K. Morokuma, G.A. Voth, P. Salvador, J.J. Dannenberg, V.G. Zakrzewski, S. Dapprich, A.D. Daniels, M.C. Strain, O. Farkas, D.K. Malick, A.D. Rabuck, K. Raghavachari, J.B. Foresman, J.V. Ortiz, Q. Cui, A.G. Baboul, S. Clifford, J. Cioslowski, B.B. Stefanov, G. Liu, A. Liashenko, P. Piskorz, I. Komaromi, R.L. Martin, D.J. Fox, T. Keith, M.A. Al-Laham, C.Y. Peng, A. Nanayakkara, M. Challacombe, P.M.W. Gill, B. Johnson, W. Chen, M.W. Wong, C. Gonzalez, J.A. Pople, Gaussian 03, Revision C.02, G. Inc. (Ed.), Wallingford CT 2004.
[47] B.H. Besler, K.M.M. Jr., P.A. Kollman, Atomic charges derived from semiempirical models, Journal of Computational Chemistry, 11 (1990) 431 - 439.
[48] W.L. Jorgensen, J. Chandrasekhar, J.D. Madura, Comparison of simple potential functions for simulating liquid water, Journal of Chemical Physics, 79 (1983) 926 - 935.
[49] J.C. Phillips, R. Braun, W. Wang, J. Gumbart, E. Tajkhorshid, E. Villa, C. Chipot, R.B. Skeel, L. Kalé, K. Schulten, Scalable molecular dynamics with NAMD, Journal of Computational Chemistry, 26 (2005) 1781 - 1802.
[50] W. Humphrey, A. Dalke, K. Schulten, VMD - Visual Molecular Dynamics, Journal of Molecular Graphics, 14 (1996) 33 - 38.
[51] R. Allen, J.P. Hansen, S. Melchionna, Molecular dynamics investigation of water permeation through nanopores, Journal of Chemical Physics, 119 (2003) 3905 - 3919.
[52] M.G. Martin, J.I. Siepmann, Transferable potentials for phase equilibria. 1. United-atom description of n-alkanes, Journal of Physical Chemistry B, 102 (1998) 2569 - 2577.
[53] A.I. Schäfer, I. Akanyeti, A.J.C. Semião, Micropollutant sorption to membrane polymers: A review of mechanisms for estrogens, Advances in Colloid and Interface Science, 164 (2011) 100 - 117.
[54] G.M. Torrie, J.P. Valleau, Monte Carlo free energy estimates using non-Boltzmann sampling: Application to the sub-critical Lennard-Jones fluid, Chemical Physics Letters, 28 (1974) 578 - 581.
[55] S. Kumar, J.M. Rosenberg, D. Bouzida, R.H. Swendsen, P.A. Kollman, The weighted hisogram analysis method for free-energy calculations on biomolecules. I. The method, Journal of Computational Chemistry, 13 (1992) 1011 - 1021.
[56] B. Roux, The calculation of the potential of mean force using computer simulations, Computer Physics Communications, 91 (1995) 275 - 282.
[57] B. Efron, R.J. Tibshirani, An introduction to the bootstrap, Chapman & Hall, New York, 1993.
[58] R. Schmid, A.M. Miah, V.N. Sapunov, A new table of the thermodynamic quantities of ionic hydration: values and some applications (enthalpy-entropy compensation and Born radii), Physical Chemistry Chemical Physics, 2 (2000) 97-102.
[59] R.R. Sharma, R. Agrawal, S. Chellam, Temperature effects on sieving characteristics of thin-film composite nanofiltration membranes: pore size distributions and transport parameters, Journal of Membrane Science, 223 (2003) 69 - 87.
[60] O. Beckstein, M.S. Sansom, A hydrophobic gate in an ion channel: the closed state of the nicotinic acetylcholine receptor, Physical Biology, 3 (2006) 147 - 159.
[61] R. Malaisamy, A. Talla-Nwafo, K.L. Jones, Polyelectrolyte modification of nanofiltration membrane for selective removal of monovalent anions, Separation and Purification Technology, 77 (2011) 367 - 374.
[62] S.U. Hong, R. Malaisamy, M.L. Bruening, Separation of fluoride from other monovalent anions using multilayer polyelectrolyte nanofiltration membranes, Langmuir, 23 (2007) 1716 - 1722.
[63] S.U. Hong, R. Malaisamy, M.L. Bruening, Separation of fluoride from other monovalent anions using multilayer polyelectrolyte nanofiltration membranes, Langmuir, 23 (2007) 1716 - 1722.
[64] L.A. Richards, M. Vuachère, A.I. Schäfer, Impact of pH on the removal of fluoride, nitrate and boron by nanofiltration/reverse osmosis, Desalination, 261 (2010) 331 - 337.

**Table Captions**

TABLE 1: Properties of hydration for each ion in bulk water including hydrated radius and average coordination number

TABLE S1: Optimized ion parameters necessary for pore simulations from the literature for fluoride and chloride[44], and developed by *ab-initio* techniques for nitrate and nitrite ("--" is non-applicable)

**Figure Captions**

FIGURE 1: Side-view representation of model system with 0.1M NaF and $R_{eff}$ = 3.3 Å. Light grey region is a volume representation of water; green ions are fluoride ($R_{ion,fluoride}$ = 1.3 Å[41]); yellow ions are sodium ($R_{ion,sodium}$ = 1.0 Å[41]).

FIGURE 2: Impact of pore size on the free energy of fluoride. (A) Free energy profile of fluoride entering pores of different sizes (center of pore is Z = 0). (B) Maximum energy barrier at different pore sizes.

FIGURE 3: Coordination number of fluoride as a function of distance in the Z-direction from bulk water into the pore for each pore size (center of pore is Z = 0).

FIGURE 4: Representation of a fluoride ion (green) at the center of the pore (Z = 0) and surrounding water for different pore sizes.

FIGURE 5: Free energy profiles (A and B) and coordination number versus distance (C and D) of different ions for two pore sizes, (A and C) Reff = 3.3 Å and (B and D) Reff = 4.3 Å (center of pore is Z = 0)

FIGURE 6: Decomposition of free energy profile with a surface charge of -0.1 $C.m^{-2}$ (applied to top membrane surface only) for fluoride with (A) $R_{eff}$ = 3.3 Å and (B) $R_{eff}$ = 4.3 Å (center of pore is Z = 0).

FIGURE S1. Generic representation of molecules to illustrate the parameterized terms shown in Table 1 (adapted from[45]). Fluoride and chloride involve only one atom (atom 1), nitrite includes one central N and two O (atoms 1, 2, 3), and nitrate has one central N and three O, with the central N out-of-plane (atoms 1, 2, 3, 4). Atom 5 represents any non-bonded atom in the system.

FIGURE S2: Ion behavior in bulk water. (A) Radial distribution function (RDF) for each ion in bulk water. RDF indicates the variation of oxygen (in water) density with distance from the center of the ion, and the size of the hydration shells are defined by the minima of the RDF function. Overlay schematic shows fluoride and its associated first hydration shell ($R_{hyd,fluoride}$ = 3.4 Å), which is defined by the first RDF minima. (B) Distribution of instantaneous coordination numbers. The probability of each ion having a given coordination number is shown as determined from their relative frequencies within the bulk simulations.



**Table 1**

| Parameter | Fluoride | Chloride | Nitrate | Nitrite |
|---|---|---|---|---|
| Ionic Radius, $R_{ion}$ (Å)* | 1.3[41] | 1.8[41] | 3.0 | 3.0 |
| Hydrated Radius, $R_{hyd}$ (Å)† | 3.4 | 3.8 | 5.1 | 5.0 |
| Average Coordination Number (--) | 6.5 | 7.1 | 15.5 | 12.7 |
| Target Hydration Free Energy (kcal.$mol^{-1}$) | -119.7[58] | -89.1[58] | -71.6[41] | -78.8[41] |
| Simulated Hydration Free Energy (kcal.$mol^{-1}$) | -119.7[44] | -89.6[44] | -71.5 | -79.1 |

* For nitrate and nitrite, $R_{ion} = b_{N\text{-}O}$ (1.22 Å) + $R_{ion,oxygen}$ (1.77 Å)
† For nitrate and nitrite, $R_{hyd} = b_{N\text{-}O}$ (1.22 Å) + $RDF_{min}$

**Table S1**

| Parameter | Fluoride[44] | Chloride[44] | Nitrate | | Nitrite | |
|---|---|---|---|---|---|---|
| | | | N | O | N | O |
| Partial Charges | -1 | -1 | 1.0323 | -0.677 | -0.058 | -0.471 |
| Non-bonded: $r_{min/2,ij}$ (Å) | 2.303 | 2.513 | 1.850 | 1.900 | 1.850 | 1.900 |
| Non-bonded: ε (kcal.$mol^{-1}$) | 0.0033 | 0.0356 | -0.200 | -0.200 | -0.200 | -0.200 |
| Bond length, b (Å) | -- | -- | N-O: | 1.2268 | N-O: | 1.2254 |
| Bond force constant, $k_b$ (kcal.$mol^{-1}$.$Å^{-2}$) | | | N-O: | 425 | N-O: | 264 |
| Angle stretch, θ (deg) | -- | -- | O-N-O: | 120 | O-N-O: | 117 |
| Angle force constant, $k_\theta$ (kcal.$mol^{-1}$.$rad^{-2}$) | | | O-N-O: | 110 | O-N-O: | 27 |
| Improper torsion, t (deg) | -- | -- | N-O-O-O: | 0 | -- | |
| Improper force constant, $k_t$ (kcal.$mol^{-1}$.$rad^{-2}$) | | | N-O-O-O: | 163 | -- | |

The Importance of Dehydration in Determining Ion Transport in Narrow Pores
Richards, L. A. , Schaefer, A. , Richards, B. S. & Corry, B. 11-Jun-2012 In : SMALL. 8, 11, p. 1701-1709.

**Figure 1**

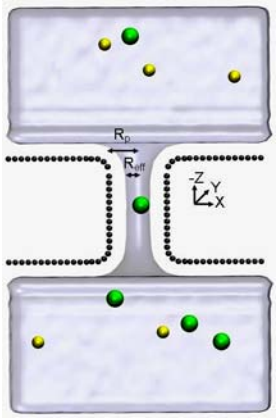




**Figure 2**

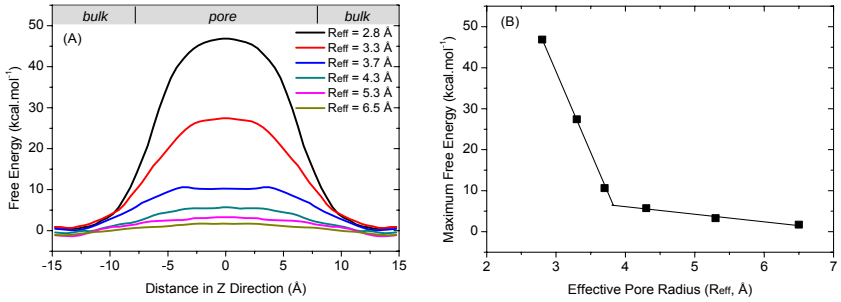

**Figure 3**

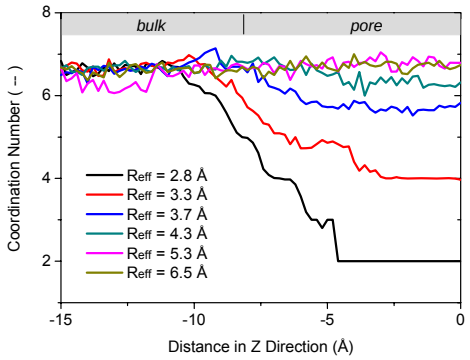




**Figure 4**

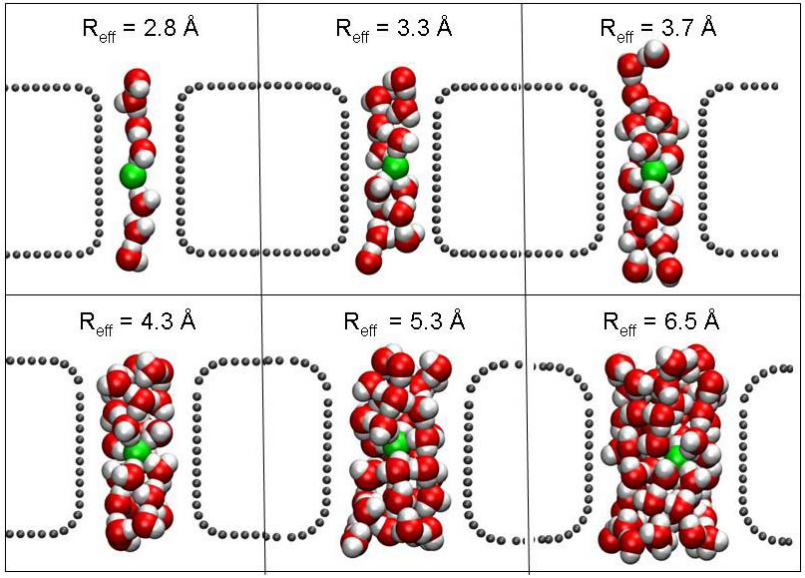

**Figure 5**

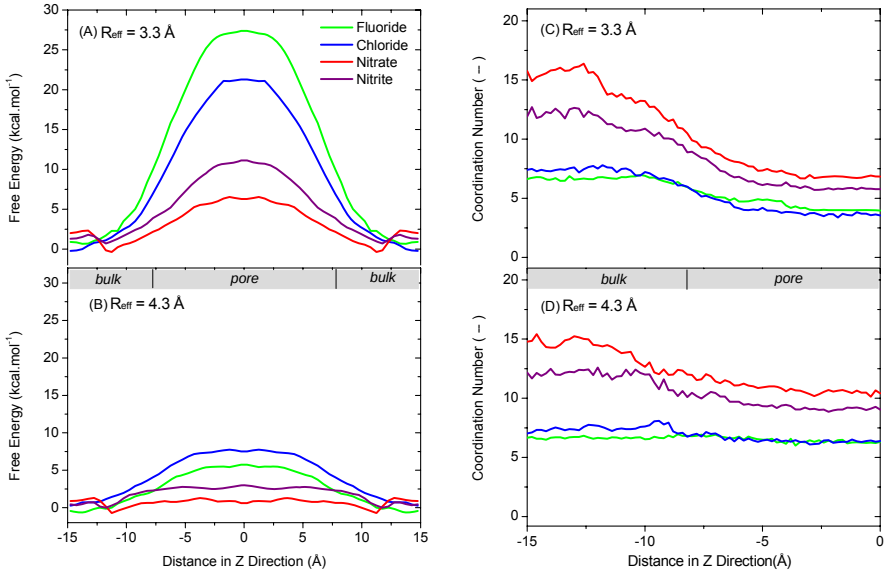




**Figure 6**

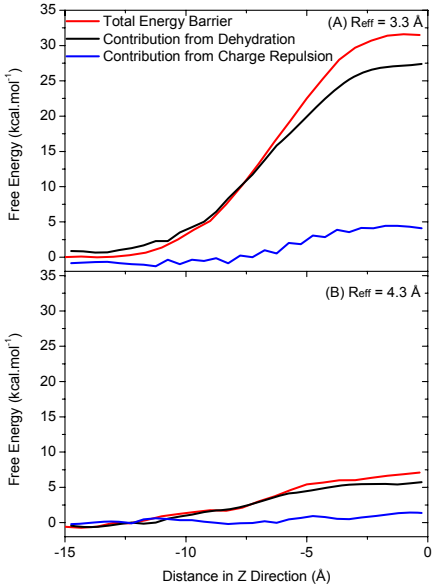

The Importance of Dehydration in Determining Ion Transport in Narrow Pores
Richards, L. A. , Schaefer, A. , Richards, B. S. & Corry, B. 11-Jun-2012 In : SMALL. 8, 11, p. 1701-1709.

**Figure S1**

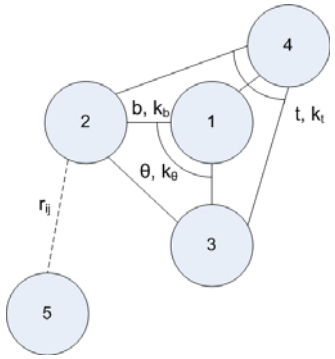




**Figure S2**